ADVANCED ENGINEERING MATERIALS
www.aem-journal.com

Defect-Free Sound Insulator Using Single Metal-Based Friction Stir Process Array

Yuqi Jin, Teng Yang, Narendra B. Dahotre, Arup Neogi, and Tianhao Wang**

Metals are excellent conductors for phonon transportation such as vibration, sound, and heat. Generally, metal sound insulators require multimaterial structure or defects and unimetal sound insulators are challenging. Therefore, a design of a defect-free sound insulator made by single alloys with multiple friction stir processes (FSPs) is proposed. Periodic friction stir processing can induce superlattice-like local mechanical properties' modifications. By experimental acoustic characterization, it is observed that FSP can introduce clear acoustic–elastic property contrast on an aluminum plate by the presence of stir zone and heat-affected zones. In numerical simulations, the signature FSP-induced property profile is periodically and parallelly arranged on a long aluminum plate. The transmission gap frequencies are present on the frequency spectrum with the sound propagation direction perpendicular to the FSP paths. Disorder offsets on FSP periodicity are further introduced. Anderson localization is found on a resonance frequency, which provides −11 dB sound reduction by an exponential decay. Due to the finite design length, the slight disorder can also enhance sound insulation in the periodic transmission gap frequency. With analysis and comparison with different configurations, the best performance in the models can achieve −30 dB sound insulation in the 350 mm-long aluminum alloy plate with 14 parallel FSPs.

1. Introduction

Metals are common structural materials owing to their excellent and tunable mechanical properties. Meanwhile, metals are also decent conductors for vibrations, sound, and heat. However, in many applications, nonuniform vibrational waves or high-strain-rate periodic stresses can induce or initiate significant failure on the metallic structures of metals and alloys during long-term service, for example, fatigue damages,[1] stress corrosion,[2] and even strong embrittlement.[3] Furthermore, in metal-to-metal joints[4] and dissimilar metal welds,[5] vibrational waves can cause more premature and substantial damage due to impedance mismatch and cavitation or internal reflecting standing waves.[4,5] Industries have focused on vibrational/sound isolation by damping using rubber mounting (**Figure 1**A),[6] utilizing the nonlinear effective stiffness of structural materials,[7] or design optimization using liquid cavities,[8] to prevent mechanical failure. Those designs are practically valuable and commonly used. But the requirements to introduce additional materials still increase the manufacturing challenges. Alternate approaches include the design of periodic structures or metastructures by fabricating hollow phononic crystal structures on the metal plates to isolate the sound or vibration by its bandgap[9] at the relevant frequencies (Figure 1B). Although the current developing topological optimization[10] can realize the phononic crystal structures with less strength loss, hollow structures on structural applications still need to be convinced by the practical applications. In this study, we introduce a simple and unique approach using a periodic array of friction stir processing on an aluminum plate to cut off the vibrational energy in a bulk structure without introducing any additional materials and hollow defects (Figure 1C). Due to the limitation of large-scale commercialized manufacturing tools, the demonstration is performed at ultrasonic frequency. The design configurations can be scaled up to the vibration frequency range with proper tool size modifications.

Friction stir processing (FSP) (as schematic shown in **Figure 2**A) was invented around 2000.[11] It is a solid-state manufacturing process for localized and continuous modification of mechanical properties in metal/alloy materials. FSP has been broadly applied for fatigue prevention,[12] crack repairing,[13] and local work hardening[14] applications.

Y. Jin, A. Neogi
Department of Physics
University of North Texas
Denton, TX 76203, USA
E-mail: yuqijin@my.unt.edu

Y. Jin, T. Yang, N. B. Dahotre
Center for Agile and Adaptive Additive Manufacturing
University of North Texas
Denton, TX 76207, USA

T. Yang, N. B. Dahotre
Department of Materials Science and Engineering
University of North Texas
Denton, TX 76207, USA

T. Wang
Energy and Environment Directorate
Pacific Northwest National Laboratory
Richland, WA 99352, USA
E-mail: tianhao.wang@pnnl.gov

The ORCID identification number(s) for the author(s) of this article can be found under https://doi.org/10.1002/adem.202300206.

DOI: 10.1002/adem.202300206

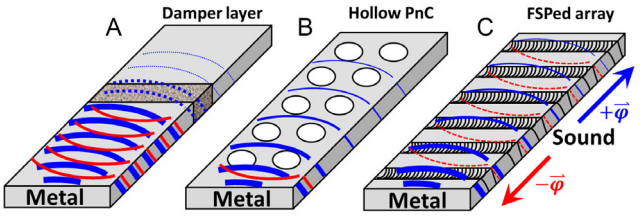

Figure 1. Illustrational drawing of the typical sound isolation methodologies in metal plates and the proposed method in this study. A) Introducing a damper layer between two metal plates using rubber or fluidic cavities. B) Using the transmission gap of a hollow scatter phononic crystal. C) Superlattice-like FSP array (periodic property modifications) with spatial randomness using coherence backscattering for destructive interference. $+\vec{\varphi}$ and $-\vec{\varphi}$ indicate the forward and backward propagations of sound wave.

Utilizing the advantage of friction stir-based manufacturing, the stir zone (SZ) of FSP yields void-free, uniform, and isotropic mechanical properties.[15] Based on the processing parameters and material chemical compositions, the processed regions can be effectively hardened or softened in terms of both effective elasticities and plasticities[16] with the refined equal-axial grained microstructure and embedded residual stresses.[17] In this study, we applied a linear FSP path array on an aluminum plate to introduce periodic and superlattice-like mechanical properties contrasts due to the presence of the SZs and their surrounding heat-affected zones (HAZs). In the presence of periodic FSP modifications, clear transmission and gap frequency ranges can be observed for sound waves propagating through the plate in the direction perpendicular to the FSP array. Utilizing the finite length of the periodic FSP plate, slight randomness introduced to the periodicity can lead to Anderson localization[18] leading to stronger noise isolation with respect to the transmission gap relative to a perfect periodic FSP array.

In a disordered material system, Anderson localization (strong localization) can be achieved when wave travel and its diffusion is destructively interfered due to coherent backscattering.[18] This wave phenomenon has been reported in photonic,[19] electronic,[20] and phononic[21] systems. In phononic systems, due to the better fabrication flexibility, Anderson localization was realized in elastic waves,[22] sound waves,[23] and even heat[24] using 1D,[25] 2D,[23] and 3D[26] structures. In 2D systems, Anderson localization was commonly introduced into a periodic system by breaking the periodicity of the phononic crystal systems.[24] However, due to the physical nature of the periodic phononic structures, the periodicity of the phononic crystals is passively structured with a fixed design configuration. Thus, the disorder was introduced to the scatterers by modifying its sizes, materials, or orientations.[23] The constant periodicity of the PnC structure offers relatively fixed frequencies of the transmission and gap bands.[27] In 1D phononic systems, the common approach to achieve Anderson localization was to use randomized periodicity on the superlattice structure.[24] However, the disorder on periodicity can eliminate the presence of the bandgap which originally appeared without disorders. For making a sound insulator, such as the proposed FSP structure in this study, we select a similar approach as literature for the design of the 1D periodic system with the disorder on periodicity. Furthermore, the balance between the degree of disorder and the presence of the periodic bandgap was analyzed to find a better sound insulation performance.

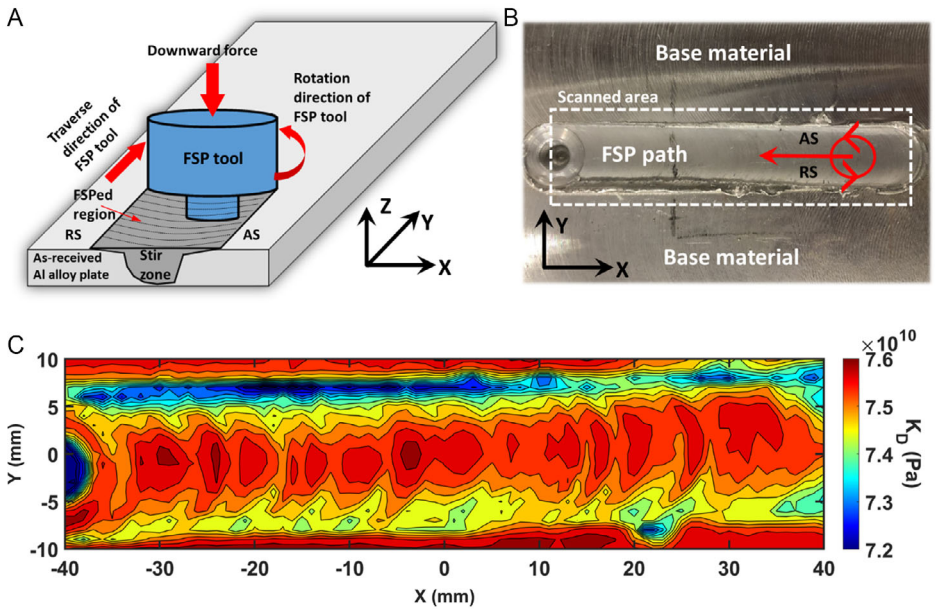

Figure 2. Experimental acoustic elastography on a single-track friction-stir-processed AA2024 workpiece for obtaining the K_D profile over the various zones on the sample: A) Illustrational drawing of the typical FSPs. AS and RS refer to the advancing side and retreating side. B) Macroscopic optical image of the FSP workpiece experimentally scanned in the work. C) Effective bulk modulus elastography on the selected region in (B) in terms of the effective bulk modulus distribution showing SZ, HAZs, and based material regions.

2. Experimental Characterization on a Single FSP Path

On a rolling processed aluminum alloy (AA) plate, we experimentally performed a friction stir processed path, as Figure 1A illustrates. The detailed processing parameters are listed in the Experimental Section. On the product (Figure 2B), we obtain an FSP path with approximately uniform width and depth beside the pinhole at the end of the path. Due to the long-time friction-induced preheating, a curvature flashing edge was observed at the starting point. For a combined rotational and linear motion, the retreating side on the left (relative to the FSP path direction) has slightly more flashing materials on the path edge than the side advancing from the right. Additional polishing and cutting are needed to remove flashing edges and the end-point hole for better performance in acoustic applications.

To understand the modification of the physical properties via FSP in the view of an acoustic wave, we performed acoustic effective bulk modulus elastography on the FSP workpiece after polishing the flashing edges shown in Figure 2C. Effective bulk modulus, also called dynamic bulk modulus K_D, is a frequency-dependent variable based on the static bulk modulus. The effective bulk modulus value includes the contribution of the microstructure size and the magnitude of residual stresses.[28] It is considered a suitable elastic constant representing the response of high-frequency vibrations or sound. The elastographic scanned area is highlighted in Figure 2B as the dashed box. The 2D map presents the distribution of effective bulk modulus, which are self-averaged values over the entire wave propagation direction (thickness of the plate) on the sample. Unlike optical photograph (Figure 2B), elastography (Figure 2C) clearly distinguishes varying property zones over the FSP path in the view of acoustic waves. With respect to the central line of the FSP path ($Y = 0$ mm), a stronger decrease in K_D is observed within the HAZs on the advancing side (AS) ($Y = 5$ mm) compared to the retreating side (RS) ($Y = -8$ mm), which induced a sharper transition between the SZ and HAZ. Around the starting point on the path ($X = 20$–40 mm), a slight asymmetricity present on the SZ represents a higher K_D on the AS. On the remainder of the path length, the K_D values on SZ were approximately symmetric. The unaffected base material shows a constant distribution of elastography K_D at the two edges. The averaged value of K_D on the *Y*-axis along the *X*-axis profile is summarized and presented in **Figure 3**A. Between the SZ and HAZs, the existence of thermomechanical affected zones (TMAZs) is worth mentioning. Due to the narrow width and small microstructure of the typical TMAZs, the TMAZs have weak potential to provide strong modification of the sound wave propagation behavior at the selected operating frequency. The existence of TMAZs is considered as to the boundary between the SZ and HAZs in this study. Hence, in the following text, the existence of TMAZs is not specifically mentioned. The TMAZs have no assigned regions in the illustration of the numerical simulations of the sound insulator. Although the property zones have distinguishable elastography features (Figure 2C), the transition between the zones still is smooth in the profile due to the long sound wavelength. The smooth transition reduces the impedance mismatch between the property zones. The smooth transition is suitable for acoustic applications when the sound propagates perpendicular to the FSP path. In the numerical simulation model, we specifically define the K_D profile into five regions, including two base material zones, 2 HAZs, and 1 SZ.

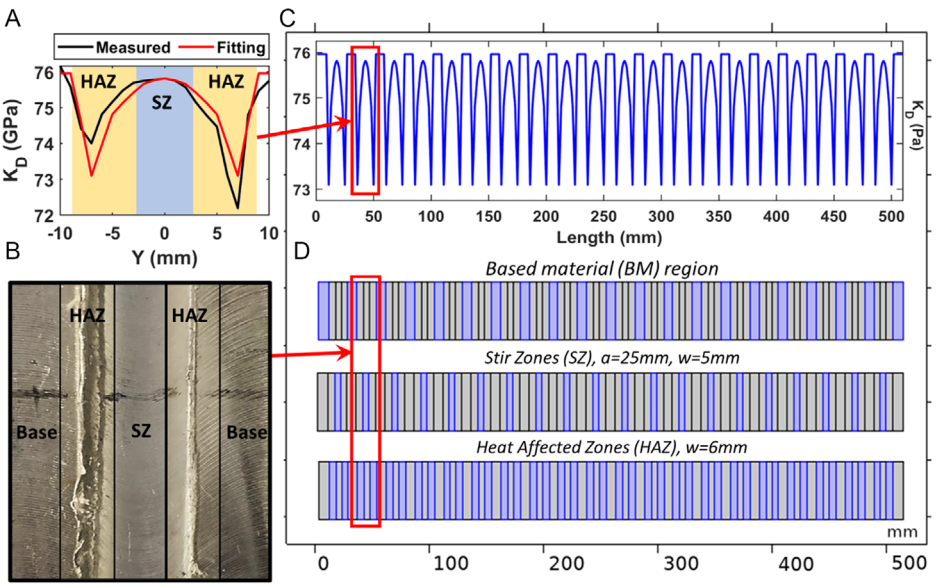

Figure 3. The design of the proposed sound insulator model of the perfect periodic arrangement on the FSP array: A) Averaged transverse direction effective bulk modulus profile along the longitudinal direction from the experimentally scanned FSP workpiece (black line). Red line indicates the symmetric curve fitting profile, which is input into the numerical simulations for the proposed design of sound insulation in the following sections. B) Illustration of the different regions on the FSP path on the macroscopic optical image. C) Complete effective bulk modulus profile of the perfect periodic 20 FSP array case in the numerical simulation. D) Illustration of the size and locations of the various zones of the ideal periodic FSP array in the numerical simulation model.

The 5 zones are united as 1 unit period in the proposed superlattice structure. Anderson localization can be introduced by assigning random offset on the periodicity to achieve sound insulation. The acoustic insulator is designed by translating the experimentally obtained K_D profile into a curve-fit symmetric K_D profile (Figure 3A red curve) as the K_D input in the acoustic wave propagation behavior simulations in the following sections. As the elastograph (Figure 2C) shows, the K_D values along the FSP track were not uniform. The beginning region of the track presents lower K_D due to the additional heat input. Hence, in practical case, the beginning and ending regions of the FSP tracks need to be cut off to maintain the uniformity of the superlattice structure.

In principle, friction stir processing significantly modifies microstructure and stores residual stresses that change the dynamic bulk modulus K_D at the processed zones and the surrounding regions. At the operating frequency in the study, the effective wavelength in aluminum is about 7.5 mm. The typical microstructure size after FSPed aluminum is less than 50 μm in SZ. In base material and HAZs, the typical size of the grain is less than 500 μm. Compared with the wavelength and microstructure size, Rayleigh scattering is not significant. Furthermore, the grain size deviation can induce dispersion effect that results in out-of-phase interference on short acoustic pulse. However, with monochromatic wave source with normal incidence, the dispersion is not considered to have significant impact on the sound insulation performance of the proposed design. In terms of acoustic properties, the metallic crystal orientations can slightly deviate the speed of sound. However, in practical, the plate before and after FSP are both polycrystalline samples. The different phases and orientations provide different speed sounds inside the samples which effectively provide approximately consistent speed of sound values. Hence, the experimental elastograph (Figure 2C) was majorly contributed by the existence of residual stresses instead of the contribution from the grain sizes.

3. Design

The first step to realize the FSP sound insulator is to introduce periodic and parallel FSP paths on a 510 mm-long and 50 mm-wide aluminum plate. A sound wave around 0.9 MHz was selected as the operating wave for the performance demonstration as it's considered a long-enough wavelength to eliminate the microstructure-induced dispersion effect.[29] It also fits the fundamental frequency of the commercially available air-coupled acoustic piezoelectrical transducers. A total of 20 FSP parallel paths were introduced on the long aluminum plate along the width direction. The overall assigned K_D profile of the 20 FSP paths is shown in Figure 3C in the numerical simulation model. The model was assembled from individual and comparable FSP paths (Figure 3B), as illustrated in Figure 3D. In the perfect periodic case, the fixed periodicity was 25 mm. In each unit period, 1 SZ with a 5 mm width and 2 HAZ with a 6 mm width was placed in the center. The remaining unit cell length was assigned as base material equally distributed at two side edges of the cell as the region connecting the periods. The design of the proposed superlattice structure is obviously different from the conventional 1D phononic crystal due to the existence of two HAZs in unit cell and the lack of sharp lattice/scatterer interface. The conventionally calculated dispersion relation cannot well describe the transmission behavior of the proposed design without thorough theatrical studies and verifications. While designing a sound insulator with normal incidence, the frequency selection was based on numerically simulated transmission spectrum instead of calculating dispersion relation in this study. In the transmission simulation, longitudinal acoustic waves were excited at the plate's left side edge and received at the right edge. The source wave was performed a frequency sweeping from 0.82 to 0.92 MHz. In the aperiodic arrangement, we introduced 20 offsets of the FSP paths with a standard deviation σ at 0.3, 0.5, 1, and 3 mm using the randomized number-generating program.[23] On each aperiodic case, 30 transmissions from 5 models were obtained with different randomized offset arrays with fixed standard deviation. The transmission profiles and frequency spectrums presented in the following section are all averages over the same standard deviation with ±0.5 kHz ensembles.

4. Results and Discussions

Figure 4A presents the summary of the frequency spectra obtained from the numerical simulations. In the reference case (solid black line: plain plate without FSP), the perfect periodic case (green line) clearly illustrated a transmission gap between 0.86 and 0.87 MHz. In the rest of the frequency spectra, the ideal periodic system shows sufficient transmission compared to the aperiodic cases. In the transmission frequency range, between 0.82 and 0.86 MHz, only the $\sigma = 3$ mm case has strong enough disorder to provide sufficient transmission drop. The spectrum of $\sigma = 3$ mm shows significant transmission reductions at 0.825, 0.835, and 0.85 MHz, which are not clearly presented in the other aperiodic cases. At 0.85 MHz, one of the resonance frequencies of the periodic case, the $\sigma = 3$mm aperiodic model, shows exponential decay (linear decay on a decibel scale) along the wave propagation direction (Figure 4B), which is about −10 dB sound insulation. On the contrary, the transmission intensity (green line) shows a negligible decrease on the resonance of the periodic case. The transmission profile on the aperiodic case (red line) proves the existence of Anderson localization on the aperiodic system when the $\sigma = 3$ mm with 20 FSP paths.

Noted that, in a phononic crystal, the transmission gap is defined to appear when the length approached infinity. In a finite-length periodic structure, the stop band presents as the certain transmission decays. For example, in the periodic case, the transmission decay of the stop band is between 0.86 and 0.87 MHz. Since the disorder in the aperiodic cases was introduced to vary the periodicity, the destruction of the periodicity induces a reduced transmission gap. For the perfect periodic system, with the standard deviation ranging from $\sigma = 0.3$ mm to $\sigma = 3$ mm, we observe a significant reduction in transmission when the disorder is substantial in the transmission frequency range. However, the sound insulation performance was better when the standard deviation of the disorder was smaller which provides additional decay at the transmission gap frequency. As the acoustic pressure distribution maps (Figure 4C) illustrate,

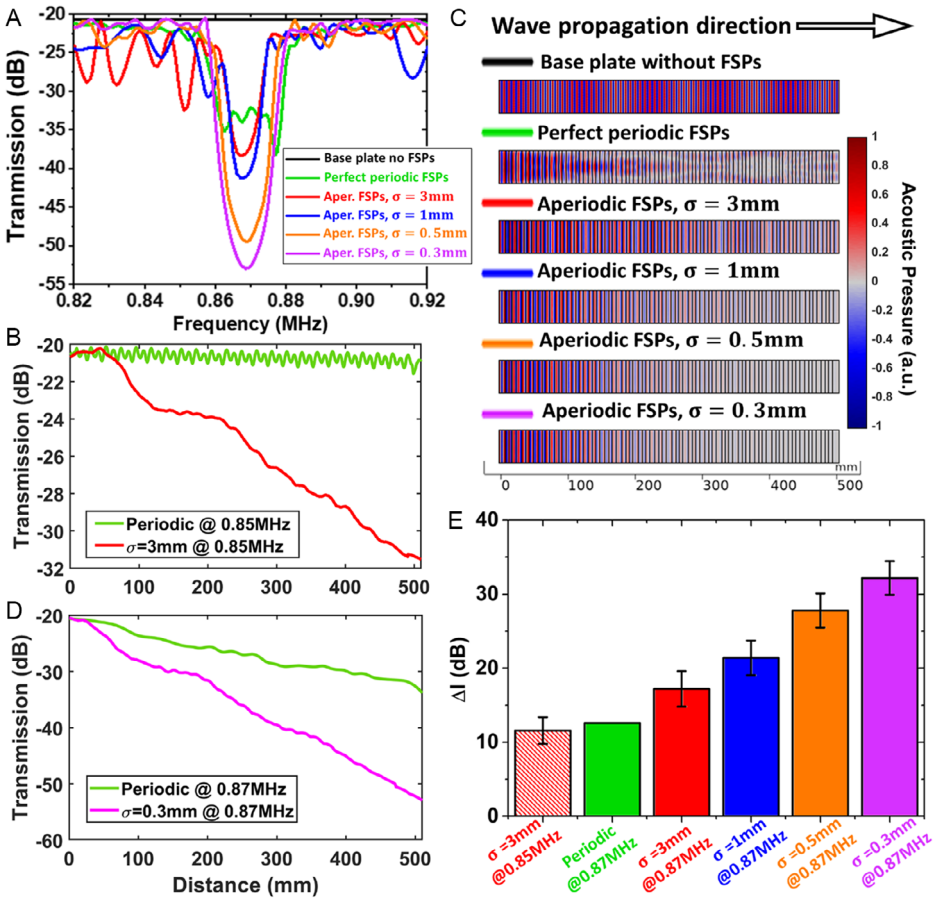

Figure 4. Numerical simulation results: A) Summary of the obtained transmission frequency spectrums including all the configurations. The frequency spectrums on the aperiodic cases were the averaged spectrums over the different models with different disorder combinations but the identical standard deviations. B) Transmission profiles over the length of the plate along the perpendicular direction of the FSP path direction, in the periodic configuration and aperiodic configuration with $\sigma = 3$ mm at one resonance frequency of the periodic configuration. C) Acoustic pressure maps on the models with different FSP arranging configurations. D) Transmission profiles over the length of the model in the periodic configuration and aperiodic configuration with $\sigma = 0.3$ mm at the transmission gap frequency of the periodic configuration. E) Summary of the sound insulation performance in terms of intensity reduction with 510 mm sample and 20 FSP paths in the proposed numerical simulation models.

at 0.87 MHz, the acoustic wave is barely transmitted in the aperiodic system when the standard deviation of the disorder is at 1, 0.5, and 0.3 mm. From the comparison between the periodic and aperiodic configurations, the strongest sound propagation reduction with $\sigma = 0.3$ mm results in a -32 dB decrease compared to the plain plate transmission. It was contributed by the constructive effects with periodic structures providing transmission gap and disorder-induced Anderson localization. In Figure 4C, the transmission profiles from the periodic system and aperiodic with $\sigma = 0.3$ mm case are presented and compared with the exponential decay presented in both cases along different slopes. Note that the transmission profile on a finite periodic structure in the transmission gap is originally equipped with exponential decay. Therefore, the presence of Anderson localization in the transmission frequency referred to in the previous paragraph can be confirmed. By comparing the two curves in Figure 4D, the additional sound decay of about -22B (depicted on the pink line) was contributed by introducing the disorder-induced Anderson localization effect at $\sigma = 0.3$ mm.

In Figure 4E, a summary of the sound insulation performance of the proposed structure is presented at varying design configurations. The error bars indicated the standard deviation of the transmission intensity difference over the statistical ensembles. In the case of a strong disorder $\sigma = 3$ mm, the presence of Anderson localization results in an 11 dB transmission reduction at the resonance frequency (0.85 MHz) with 20 periods of the proposed structure. It is not a strong enough isolation compared to the transmission reduction at the transmission gap in the periodic case. On the contrary, the disorder-induced additional transmission decay in the gap frequency (0.87 MHz) implies an obvious inverse proportional relationship with respect to the transmission frequency, which shows that the total transmission decay is more significant with weaker randomness (from green bar to pink bar). Based on the transmission results obtained from the numerical simulation in **Figure 5**A, we further estimated the localization length for the proposed structure using the expression:[23] $L^{-1}(f) = \left\langle \frac{2}{d} \ln \frac{I_0}{I(d,f)} \right\rangle$, where d is the sample length, the distance in the present work in the crystal along the wave

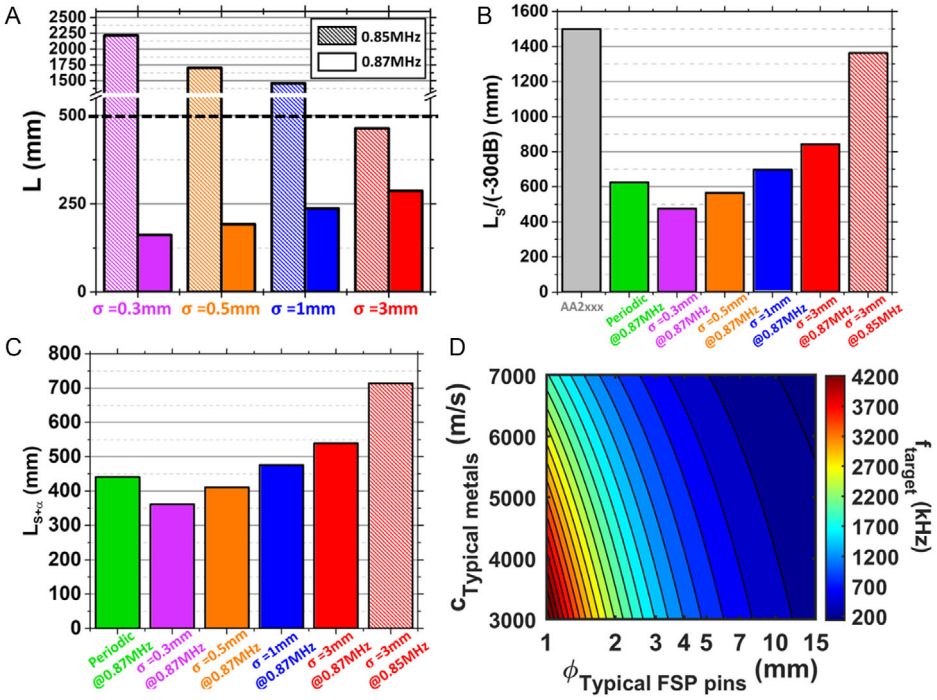

Figure 5. Discussion on the performance and potential capability of the proposed design: A) Estimated localization length of the four disordered cases at 0.85 and 0.87 MHz based on the numerical simulation results in Figure 4. B) Comparison with the different simulated cases for estimating required sample lengths on the studied models for −30 dB sound insulation. The gray reference bar indicated the estimated length of AA2xxx alloy without an FSP path but with a practical attenuation coefficient obtained from the literature. The attenuation was not considered in the other cases with FSP paths. C) The estimated required sample lengths on the studied models for −30 dB sound insulation, including the attenuation coefficient of AA2xxx in all the studied cases for comparison. D) Potential sound insulation frequency range with reasonable scale-up or scale-down of the proposed design with additional modifications based on the available FSP tool size and FSP materials.

propagation distance. I_0 and I are the source intensity and transmission intensity. f is the operating frequency. In the transmission frequency (0.85 MHz, shadow bars), it was obvious that the estimated localization lengths on the cases $\sigma = 0.3$ mm, $\sigma = 0.5$ mm, and $\sigma = 1$ mm exceeded the sample length 510 mm in the simulation models, which agreed with frequency spectrums in Figure 4A, showing no clear transmission reduction. Only in the $\sigma = 3$ mm case, the disorder is strong enough to reduce the localization length under 510 mm. Hence, a clear transmission dip was found on the frequency spectrum at 0.85 MHz (red line Figure 4A). In the transmission gap frequency (0.87 MHz, clean bars), all four cases have estimated localization lengths under the proposed sample length. It further proves the presence of reduced transmission in the frequency spectra in Figure 4A.

In Figure 5B, we calculated an estimation plot to discuss the sample size requirement on each FSP array configuration for a −30 dB sound insulation. Generally, −30 dB is considered a decent amount of sound insulation. As a reference, on the gray bar, we include acoustic wave dissipation on AA2xxx using its attenuation coefficient α from existing literature.[30] Although the coefficient α is strongly frequency dependent in high frequency due to the microstructure, below 5 MHz, the coefficients of ultrasonic attenuation in aluminum alloy 2xxx were found to be around 10–30 dB m^{-1} dependent on the compositions and processing methods.[30] Note that the attenuation coefficient of AA2xxx is not considered in the estimations for other FSP array cases. With only the contribution from the transmission gap decay and the decay from the Anderson localization, in the FSP array cases, all the configurations can reduce the sound intensity by −30 dB within 1 m. With the assistance from the $\sigma = 0.3$ mm disorder, the pink bar shows about 150 mm shorter on the required length to achieve −30 dB insulation with respect to the system that only involved the reduction due to transmission gap from the periodic FSP array. In Figure 5C, the attenuation coefficient α of AA2xxx is taken account into the estimations for −30 dB sound insulation for all the FSP array sound insulators, which considers a situation closer to the practical case. With the additional attenuation from the aluminum alloy, the required sample lengths reduced by about 30% to block sound waves for −30 dB for the superlattice cases. Hence, at the transmission gap frequency 0.87 MHz, most of the proposed configurations can achieve −30 dB insulation within 510 mm sample length, including the periodic case and the aperiodic cases $\sigma = 0.3$ mm, 0.5 mm, and 1 mm. On the aperiodic case with $\sigma = 0.3$ mm, the estimated sample length is about 350 mm which refers to 14 periods of the FSP array. In practice, a strong mechanical property contrast phononic superlattice structure can achieve a sufficient transmission gap with 10 periods or more. With low contrast in mechanical properties, the aluminum FSP array with a minor disorder can effectively reduce noise for −30 dB with 14 periods, which is considered as decent performance.

With numerical simulations, the ideal performance of the proposed design was demonstrated. However, exact realization of the proposed design by conventional FSP requires very precise manufacturing including uniform K_D on the raw material (plate), preventing of the thermal strain of the base plate during the FSPs, avoiding the additional heat effects to the processed path during the processing, controlling of the wearing conditions of the tool pin, and so on. However, due to the mechanism of the sound insulation, Anderson localization, slight experimental errors/flaws (additional randomness) would not significantly impact the performance of the sound insulation in principle. However, the target frequency range of the proposed design potentially has a frequency shift due to the presence of experimental errors and flaws, which would be hard to avoid in future experiments. In addition, small defects commonly exist in friction stir samples. With proper parameter optimization and quality control of the tool, the presence of defects can be reduced. However, for the design of a FSP array sound insulator, the presence of small defects should not affect the performance of the sound insulator in principle. The presence of defects in the sound insulator can dissipate more acoustic energy during the propagation of the acoustic wave which effectively enhances the performance of the sound insulator. However, due to the defects deviated effective local K_D, the target operating frequency of the designed sound insulator can be potentially shifted. In future experimental studies, precharacterization of tool/parameter-dependent defects fraction of the FSP sample would be necessary to be conducted for obtaining a better prediction of the correlation between real products and corresponding numerical simulations.

In general, the proposed sound insulator design is not limited to a certain operating frequency. Proper scaling up or down can shift the operating frequency of the superlattice structure. However, the reasonable scaling needs to follow the size of the sizing FSP tools which refers to the size of the unit cell in the sound insulator. In the normalized scale, the insulation wavelength $\lambda = 1.47\phi$, where ϕ refers to the diameter of the FSP tool pin. Wavelength can be further translated into the fundamental relation $c = \lambda f$, where f indicates the target frequency of the sound wave to be blocked, and c is the speed of sound which is a material-dependent property. With the normalized relation, we summarize the flexibility for scaling up or down on the proposed structure in Figure 5D. The typically used FSP tool diameters range between 1–15 mm, in which the 1 mm tool is frequently used in microscale friction stir welding or processing (μFSP). 12–15 mm diameter tools can perform large-scale structure processing, including aerospace and automobile industries. With the background of the commercialized FSP tools and FSP feasible metals/alloys (longitudinal sound velocity in the range between 3000 and 7000 m s^{-1}), the estimated insulation frequency map shows that potential scalable FSPs sound insulators can cover the sound insulation frequency covering supersound to ultrasound range from 140 kHz to 4.25 MHz without advanced modifications on the proposed configurations. In addition, the development and research are heavily conducted on the metals' solid-state additive manufacturing,[31] such as additive friction stir deposition processing. With very different printing (deposition) parameters, different heating/cooling rates and mechanical stresses can result in strong enough mechanical properties contrast, contributed by the variations in microstructures and residual stress distributions. Such proposed defect-free and full-metal sound insulation structures are feasible to be realized by AM processing with higher geometrical flexibility.

5. Conclusion

In the present work, we designed an approach to achieve a unimetal defect-free sound insulator without the assistance of additional materials or defects. Solid-state local modification method, friction stir processing, was selected to produce line array modifications on an aluminum alloy plate. With experimentally obtained FSP-induced effective bulk modulus profile, a 20 FSP path periodic structure was tested by numerical simulation for observation of the sound wave propagation behaviors. Superlattice-like transmission band and transmission gap frequency ranges were found. The exponential decay of the resonance frequency proved the occurrence of Anderson localization. We further introduced disorder in the periodicity of the FSP array. Disorders with different standard deviations were applied to the FSP array model. In the finite length model, the sound decays faster with a more significant disorder in the transmission frequency range, but the sound decays more quickly with a weaker disorder in the transmission gap frequency range. Combined with transmission gap decay and disordered induced decay, the best performance model can provide a −32 dB sound insulation without considering the sound attenuation in aluminum alloy. A −30 dB isolation can be realized with only 14 FSP paths instead of 20 periods when considering the material-induced attenuation effect. Based on the typical FSP tool size and general FSP materials, sound insulation can be effective in the frequency range from 140 kHz to 4.25 MHz with scale-up or scale-down on the proposed configurations.

6. Experimental Section

2024-T3 aluminum alloy plates (10 mm thickness) were heat treated to 375 °C for 2 h and slowly cooled down to room temperature, and the process was applied to remove the residual stress in the as-received condition. After heat treatment, the plate was friction stir processed with an FSP tool manufactured from MP159 alloy. The detailed dimensions of the FSP tool were a shoulder diameter of 15 mm, a pin length of 5 mm, and pin root diameter of 5 mm. The FSP tool shoulder was concave, and the tool pin had threaded features. During FSP, a constant rotation rate of 150 RPM, traverse speed of 75 mm min^{-1}, and tool tilt angle of 0.5° were applied. Note that low RPM and high traverse speed can narrow down the HAZ, which allowed for a more evident physical property contrast between SZ and HAZ and better sound insulation effect which was important to serve as a unit cell in 1D phononic crystal structure. In this work, the demonstration of the FSP modification of the aluminum alloy was shown on AA2024-T3. However, the design was not limited to the specific alloy type. Certain slight modifications on the superlattice design might apply depending on the alloy selection in terms of the periodicity and operating frequency. As long as the alloy after FSP modification could have two significant HAZs and a higher K_D SZ between the HAZ, the full metal sound insulator was valid in principle.

The ultrasonic effective bulk modulus elastography of the friction-stir-processed workpiece was conducted in a glass open-top container filled with Nu-clear cutting oil. An Olympus unfocused immersion transducer with a center frequency at 1 MHz was selected to excite a broadband

pulse with a repetition rate every 2 ms during the pint-by-point raster scan with a 1 mm spatial interval and collected the reflection from the upper and lower sample surfaces. The scan was controlled by a preprepared MATLAB script operating a UR5 robotic arm. A JSR Ultrasonics DPR 500 Pulse/ Receiver was involved in being the source of the pulse source and time trigger. The collected temporal data and the time trigger were sent to Tektronix MDO 34 oscilloscope with a consistent time range window at a 1 GHz sampling rate. In the collected signals, the reflected pulses from the upper and lower surfaces of the scanned sample were located for a further calculation to obtain the dynamic (effective) bulk modulus following the equation:[29] $K_D = cZ_0\left(\frac{-1-\xi-\sqrt{4\xi+1}}{\xi-2}\right)$, where $\xi = \frac{p_1}{p_e-p_0}$, p_e is the magnitude of the emitted pulse from the transducer, p_0 and p_1 are magnitude of reflection from the upper and lower surfaces of the workpiece, c is the speed of sound in the sample, Z is the acoustic impedance of the scanned sample, and Z_0 is the reference acoustic impedance of the ambient material (Nu-clear cutting oil in this study). The experimental K_D profile from the FSP sample was repetitively assigned on the plate in the numerical simulation which contained the base material regions, SZ, and HAZs. In the initial experimental scan on the FSP sample, the identification was made by locating the SZ and base material regions. The width of the SZ approximately equaled the diameter of FSP tool pin. The base material regions on the 2 sides were distinguished at the locations in which the K_D values approximately were equal to the original material. The HAZs were the regions between the SZ and base material regions.

The numerical simulations were performed using finite-element analysis based on COMSOL Multiphysics software version 5.5. For all the studies, frequency domain studies were applied to the pressure acoustic module. A 510 mm x50mm-sized aluminum alloy plate was constructed in the model. The two long edges were set to the boundary conditions as impedance matching conditions for representing a wide enough plate to avoid internal reflection due to the spreading of the acoustic waves. The left short edge was set to the acoustic source for emitting plane waves, whereas the right-side boundary was set to sound hard boundary with a boundary probe for detecting the acoustic waves. The bulk modulus of the plate was assigned by the repeating K_D curve presented in Figure 2A. The perfect periodic case K_D the curve is presented in Figure 2C. The disorders were introduced by assigning offset on the periodicity of one entire FSP path, including a base material, HAZ, SZ, HAZ, and base material. The speed of sound was set to be a constant value obtained from the averaged value in the EBME scan $c = 6318\ \mathrm{m\ s^{-1}}$. The distinguishment of the SZ and HAZ areas in the numerical simulation was relied on the assigned bulk modulus distribution. On the perpendicular direction with respect to the welding direction, this transversal bulk modulus distribution was obtained from the curve of the fitting on the experimental scanned results (Figure 3A). The K_D profile (red line) indicated a unit cell in the proposed superlattice structure. For the periodic array case, the K_D profile was repetitively assigned on the modeled large plate along the perpendicular direction with respect to the welding direction. Along the welding direction, no spatial difference was set for maintaining a 1D phononic crystal configuration. In the numerical simulation, monochromatic longitudinal mode acoustic waves were emitted on the left side edge and received on the right edge with a frequency sweeping from 0.82 to 0.92 MHz. In the aperiodic arrangement, 20 offsets of the FSP paths were assigned with the certain standard deviation σ at 0.3, 0.5, 1, and 3 mm. Due to the long operating wavelength relative to the typical microstructure size, there was a negligible effect on the speed of sound due to Rayleigh scattering. Based on the literature, although residual stresses can change the speed of sound values in aluminum alloys, the variation is generally within 1% changes. Hence, this study did not consider the low changing rate of acoustic velocities within the small region under residual stresses. The frequency spectrums were obtained from the frequency sweeping between 0.82 and 0.92 MHz with 0.25 kHz frequency step intervals. In the models, the mesh was selected to be the automatically formed mesh by the general physics setting with the extrafine option, which offered the maximum mesh element size at 0.034 λ.

Acknowledgements

This work was supported by EFRI grant no. 1741677 from the National Science Foundation and Advanced Materials and Manufacturing Processes Institute (AMMPI) 2019 SEED grants. This work was also supported by the infrastructure and support of the Center for Agile & Adaptive and Additive Manufacturing (CAAAM) funded through State of Texas Appropriation #190405-105-805008-220.

Conflict of Interest

The authors declare no conflict of interest.

Data Availability Statement

The data that support the findings of this study are available from the corresponding author upon reasonable request.

Keywords

acoustic metamaterials, Anderson localizations, disordered arrays, mechanical property modifications, metal sound insulators, superlattices

Received: February 14, 2023
Revised: June 21, 2023
Published online: July 9, 2023

[1] M. Mršnik, J. Slavič, M. Boltežar, *Int. J. Fatigue* **2013**, *47*, 8.
[2] G. T. Flowers, F. Xie, M. J. Bozack, X. Hai, B. I. Rickett, R. D. Malucci, *IEEE Trans. Compon. Packag. Technol.* **2006**, *29*, 318.
[3] X. Yang, B. Zhang, *Int. J. Extreme Manuf.* **2019**, *1*, 022003.
[4] P. Pandurangan, G. D. Buckner, *Exp. Mech.* **2006**, *46*, 601.
[5] S.-H. Han, D.-G. An, S.-J. Kwak, K.-W. Kang, *Int. J. Fatigue* **2013**, *48*, 170.
[6] L. P. Davis, J. F. Wilson, R. E. Jewell, J. J. Roden, *NASA Marshall Space Flight Center*, Journal of Astronomical Telescopes, Instruments, and Systems, Huntsville **1986**.
[7] Y. Liu, J. Liu, G. Pan, Q. Huang, *Rev. Sci. Instrum.* **2023**, *94*, 015105.
[8] H. Murai, *U.S. Patent 6,419,213*, **2002**.
[9] J. O. Vasseur, P. A. Deymier, B. Djafari-Rouhani, Y. Pennec, A. C. Hladky-Hennion, *Phys. Rev. B* **2008**, *77*, 085415.
[10] G. Yi, B. D. Youn, *Struct. Multidiscip. Optim.* **2016**, *54*, 1315.
[11] Z. Y. Ma, *Metall. Mater. Trans. A* **2008**, *39*, 642.
[12] S. R. Sharma, Z. Y. Ma, R. S. Mishra, *Scr. Mater.* **2004**, *51*, 237.
[13] C. Gunter, M. P. Miles, F. C. Liu, T. W. Nelson, *J. Mater. Sci. Technol.* **2018**, *34*, 140.
[14] M. A. A. Anshari, M. Imam, M. Z. K. Yusufzai, V. Chinthapenta, R. Mishra, *Mater. Sci. Eng., A* **2021**, *805*, 140582.
[15] F. Hannard, S. Castin, E. Maire, R. Mokso, T. Pardoen, A. Simar, *Acta Mater.* **2017**, *130*, 121.
[16] V. Patel, W. Li, A. Vairis, V. Badheka, *Crit. Rev. Solid State Mater. Sci.* **2019**, *44*, 378.
[17] P. Staron, M. Kocak, S. Williams, A. Wescott, *Physica B* **2004**, *350*, E491.
[18] P. W. Anderson, *Phys. Rev.* **1958**, *109*, 1492.
[19] D. S. Wiersma, P. Bartolini, A. Lagendijk, R. Righini, *Nature* **1997**, *390*, 671.
[20] Z. Shi, J. Wang, A. Z. Genack, *Proc. Natl. Acad. Sci.* **2014**, *111*, 2926.
[21] Y. Ye, M. Ke, J. Feng, M. Wang, C. Qiu, Z. Liu, *J. Phys.: Condens. Matter* **2015**, *27*, 155402.

[22] S. E. Skipetrov, Y. M. Beltukov, *Phys. Rev. B* **2018**, *98*, 064206.
[23] J. Dhillon, A. Bozhko, E. Walker, A. Neogi, A. Krokhin, *J. Appl. Phys.* **2021**, *129*, 134701.
[24] T. Juntunen, O. Vänskä, I. Tittonen, *Phys. Rev. Lett.* **2019**, *122*, 105901.
[25] A. Croy, P. Cain, M. Schreiber, *Eur. Phys. J. B* **2011**, *82*, 107.
[26] G. Semeghini, M. Landini, P. Castilho, S. Roy, G. Spagnolli, A. Trenkwalder, M. Fattori, M. Inguscio, G. Modugno, *Nat. Phys.* **2015**, *11*, 554.
[27] T. Yang, Y. Jin, N. B. Dahotre, Z. Wang, A. Neogi, *Adv. Eng. Mater.* **2023**, *25*, 2201758.
[28] Y. Jin, T. Wang, A. Krokhin, T.-Y. Choi, R. S. Mishra, A. Neogi, *J. Mater. Process. Technol.* **2022**, *299*, 117301.
[29] Y. Jin, X. Wang, E. A. Fox, Z. Xie, A. Neogi, R. S. Mishra, T. Wang, *Adv. Intell. Syst.* **2022**, 2100215.
[30] K. Ono, *Appl. Sci.* **2020**, *10*, 2230.
[31] H. Z. Yu, R. S. Mishra, *Mater. Res. Lett.* **2021**, *9*, 71.